START-TO-END SIMULATIONS FOR PAL XFEL PROJECT

Yujong Kim*, DESY, D-22603 Hamburg, Germany
J. S. Oh, M. H. Cho, I. S. Ko, and W. Namkung, PAL, POSTECH, Pohang 790-784, Korea
D. Son and Y. Kim, The Center for High Energy Physics, Daegu 702-701, Korea

Abstract

At the Pohang Accelerator Laboratory (PAL), there is a 2.5 GeV S-band linac which is under operating as a full energy injector for the Pohang Light Source (PLS) storage ring. By installing a new S-band photoinjector, a new 0.7 GeV linac, and two new bunch compressors, the PLS linac can be operated as an FEL driver for the PAL XFEL project. To generate ultrashort, ultrabright, and coherent X-ray FEL sources, we should supply high quality electron beams to a long undulator. In this paper, we describe design concepts of the new injector, bunch compressors, linac layout optimization, and various start-to-end (S2E) simulations on linac optimization and jitter.

INTRODUCTION

During the nominal operation of the PLS storage ring, 2.5 GeV PLS linac is operated as a full energy injector for the ring, and its total injection time is within about 20 minutes a day. Since the PLS linac does not have any other special dedicated service, the linac can be ideally converted into the FEL driver for an X-ray FEL facility. To supply femtosecond (fs) hard X-ray FEL sources, recently, Korean government approved the PLS linac upgrade for the PAL XFEL project. Under the fundamental mode operation of the PAL XFEL facility, its tunable shortest wavelength is 3 Å, and FEL sources with more shorter wavelength can be also available by various higher harmonic generation technologies [1]. Detail FEL related parameters for the PAL XFEL project can be found in references [2] and [3], and its required electron beam parameters for 3 Å and 1 Å FEL sources are summarized in Table 1. Generally, FEL source properties strongly depend on the electron beam parameters such as slice and projected normalized rms emittances, slice rms relative energy spread, and peak current. And these parameters are mainly determined by the injector system and bunch compressors (BCs) in the FEL driving linac. Since the current 80 kV DC gun can not generate high quality electron beams, a new gun, two bunch compressors, and a new injector linac should be added to the existing PLS linac to supply required electron beams for the PAL XFEL project. However its overall modification must be minimized to reoperate the PLS storage ring within a limited period. In this paper, we propose one possible linac layout for the PAL XFEL project and describe various S2E simulation results with ASTRA and ELEGANT codes.

* E-Mail : Yujong.Kim@DESY.de, URL : http://www.desy.de/∼yjkim

Table 1: Main parameters for PAL XFEL project.

Parameter	Unit	3 Å / 1 Å
beam energy E	GeV	3.0 / 3.0
single bunch charge Q	nC	1.0 / 1.0
slice normalized rms emittance ϵ_{ns}	μm	1.5 / 1.0
slice rms relative energy spread $\sigma_{\delta s}$	10^{-4}	2.0 / 2.0
peak current I_{pk}	kA	4.0 / 4.0
undulator length for fundamental mode	m	60 / 37
undulator length for the 3rd harmonic	m	· / 23

INJECTOR FOR PAL XFEL PROJECT

Recently, by the help of a flat-top laser profile with about 9 ps (FWHM) length and about 1.5 ps rising and falling time, one BNL/SLAC/UCLA type S-band RF gun with a 14 MeV booster linac had generated high quality electron beams with a projected normalized rms emittance of about 1.2 μm for 1 nC singe bunch charge [4]. After considering two facts that slice normalized rms emittance should be smaller than 1.0 μm to generate 1 Å FEL source, and projected and slice emittances can be diluted at bunch compressors due to the microbunching instability and CSR, we determined that the PAL XFEL injector should supply much higher quality electron beams with a smaller projected normalized rms emittance [5]-[7].

This required higher quality electron beams can be generated by upgrading the BNL/SLAC/UCLA type S-band RF gun with following steps [4]: First, transverse laser profile will be improved to have a good homogeneous intensity, and longitudinal laser profile will be improved to have a good uniform flat-top shape with a shorter rising and falling time. These improvements will help in reducing emittance growth at head and tail regions due to the nonlinear space charge force [5]. Second, the maximum gradient at the cathode will be increased from current 100 MV/m to 120 MV/m which will also help in reducing space charge force effects [8]. Third, we will align laser on the cathode and correct solenoid misalignments by the beam based alignment. Fourth, several fine optimizations will be done under 120 MV/m gradient: gun RF phase optimization to get the maximum energy gain, laser pulse length optimization to control longitudinal space charge force, laser spotsize optimization at the cathode to control transverse space charge force and thermal emittance, solenoid current optimization to compensate emittance growth in gun region due to space charge force and to reduce emittance growth due to the none-zero magnetic field on the cathode [8], [9].

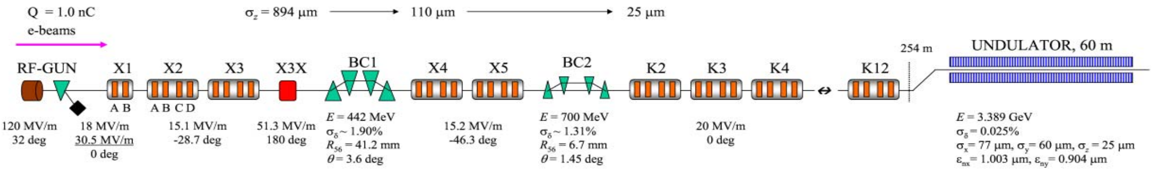

Figure 1: One possible linac layout (21JUL04 version) for PAL XFEL project.

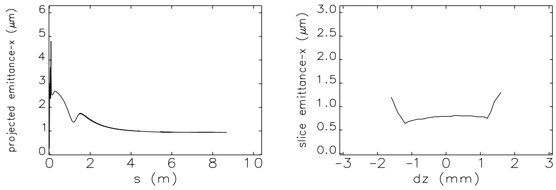

Figure 2: ASTRA simulation results on PAL XFEL injector: (left) projected normalized rms horizontal emittance up to the end of X1B, and (right) slice normalized rms horizontal emittance at the end of X1B. Here the entrance of X1A and X1B are located at 1.4 m and 5.4 m downstream from the cathode, respectively.

Fifth, we will re-compensate the second emittance growth due to space charge force in the drift space between gun and the booster linac by installing the first S-band accelerating column (X1A) at the so-called *Ferrario matching point* as shown in Figs. 1 and 2 [10]. Here, X1A has a lower gradient to satisfy the *Ferrario matching condition* and the second accelerating column (X1B) has a higher gradient to get a higher beam energy and to control Twiss parameters in X1B [10]. According to our ASTRA simulations for the PAL XFEL injector, we may generate higher quality electron beams with a projected normalized rms emittance of around 0.94 μm by following above optimization steps. Its simulation results are shown in Fig. 2, and its detail simulation conditions are summarized in Table 2.

Table 2: S2E simulation results for PAL XFEL project.

Parameter	Unit	Value
RF frequency of gun and linac	MHz	2856
repetition rate	Hz	60
gun cell number	cell	1.6
laser spotsize at cathode $\sigma_{x,y}$	mm	0.60
laser pulse length (FWHM)	ps	10
laser pulse rising and falling time	ps	0.7
normalized thermal emittance	μm	0.60
maximum longitudinal solenoid field	T	0.272
maximum gradient at the cathode	MV/m	120
gun phase from zero crossing	deg	32
accelerating gradient in X1A	MV/m	18
accelerating gradient in X1B	MV/m	30.5
X1A and X1B phase from on crest	deg	0.0
projected emittance before BC1 / BC2	μm	0.94 / 0.99
slice emittance before BC1 / BC2	μm	0.81 / 0.81
bunch length before BC1 / BC2	μm	894 / 110
beam energy before BC1 / BC2	MeV	442 / 700
projected energy spread before BC1 / BC2	%	1.90 / 1.31
slice energy spread before BC1 / BC2	10^{-5}	0.92 / 4.30
projected emittance after BC2 / LINAC	μm	1.08/ 1.00
slice emittance after BC2 / LINAC	μm	0.81 / 0.81
bunch length after BC2 / LINAC	μm	24.6 / 24.6
beam energy after BC2 / LINAC	GeV	0.70 / 3.39
projected energy spread after BC2 / LINAC	%	1.27/ 0.03
slice energy spread after BC2 / LINAC	10^{-4}	2.44 / 0.29

BC FOR PAL XFEL PROJECT

Basic bunch compressor design concepts are well described in references [7] and [11]. The same concepts are used in designing bunch compressors for the PAL XFEL project. Since dispersion is reversed inside of the S-type chicane, the chicane is generally useful in compensating the projected emittance growth [12]. But its overall CSR strength is much higher than that of the normal chicane with four dipoles because S-type chicane has two additional dipoles [12]. Specially, if current density profile and/or energy profile have a modulation before the S-type chicane, its CSR microbunching instability is stronger than that of the normal chicane [12].

To avoid slice parameter dilution due to the microbunching instability in BCs, we have adopted followings in our linac layout as shown Fig. 1: First, to reduce overall CSR strength, we choose only two bunch compressors with the normal chicane instead of S-type chicane. Second, to keep the slice rms relative energy spread at the entrance of BC2 large, we put BC2 at a low beam energy of around 700 MeV. In this case, BC2 has still a large projected rms relative energy spread of around 1.31%. Third, during compression in BCs, slice energy spread generally becomes larger to conserve the normalized longitudinal emittance. Therefore slice rms relative energy spread before BC2 can be further increased up to 4.3×10^{-5} by compressing bunch length at BC1 strongly. Since the compression factor at BC1 is high, we put BC1 at 442 MeV to avoid any beam dilution due to space charge force. Note that our linac layout can be also operated as the double chicane mode only by turning off two S-band accelerating sections (X4 and X5) and by rematching optics [5], [7]. In this case,

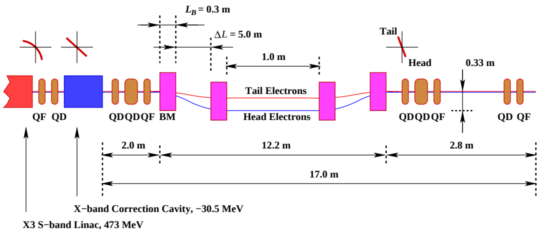

Figure 3: BC1 layout for PAL XFEL project. BC2 chicane has the same layout.

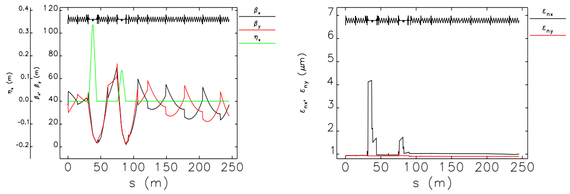

Figure 4: Twiss parameters (left) and projected emittances (right) along PAL XFEL linac.

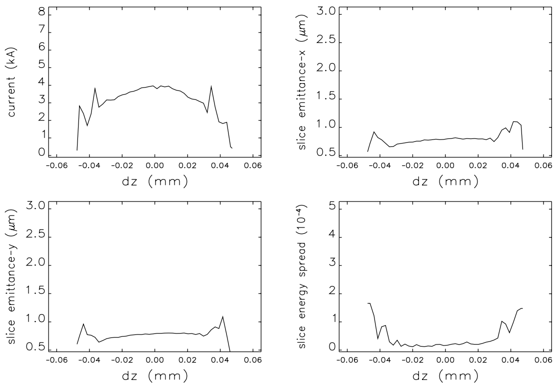

Figure 5: Slice parameters at the end of PAL XFEL linac.

microbunching instability will be effectively damped [5].

To avoid projected emittance dilution due to CSR in BCs, we have adopted followings in the PAL XFEL linac layout as shown in Figs. 1 and 3: First, to reduce CSR, we should choose a smaller momentum compaction factor R_{56} of chicane. This is possible by choosing a somewhat larger projected rms relative energy spread σ_δ [11]. After considering the emittance growth due to chromatic effect, we choose 1.90% at BC1. Second, we choose short quadrupoles around BCs to reduce emittance growth due to chromatic effect. Third, for a required R_{56}, we can reduce dipole bending angle (hence, CSR) further by using a longer drift space ΔL between the first dipole and the second one as shown in Fig. 3 [11]. Fourth, generally, CSR is weaker at BC1, and CSR becomes stronger at BC2 as bunch length is compressed. Hence, we choose a higher compression factor at BC1 and a lower compression factor at BC2 to reduce overall CSR effects in our two BCs. Fifth, we reduce CSR further by installing a 4th harmonic X-band accelerating column (X3X) before BC1 to compensate nonlinearities in the longitudinal phase space as shown in Fig. 3 [11]. Sixth, if we use a long linac between BCs, the longitudinal short-range wakefield in the linac induces a small change in the longitudinal-phase-space chirping slope at head and tail regions, where charge is low. In this case, projected emittance is increased due to over-compression at head and tail regions in BC2 [10]. Therefore we reduce the length of S-band linac between BCs to reduce the projected emittance growth at BC2. Seventh, the projected emittance dilution due to CSR can be reduced further by forcing the beam waist close to the last dipole where α-functions are zero, and β-functions are their minimum as shown in Fig. 4 [11]. Since chromatic effects becomes smaller at BC2 due to smaller σ_δ, we choose much higher β-functions at the upstream of BC2 to give strong focusing in BC2 as shown in Fig. 4(left) [11]. In this case, the projected emittance growth due to CSR can be effectively reduced at BC2.

To check performance of our linac layout, we have performed S2E simulations with ASTRA and ELEGANT codes as shown in Figs. 1 and 4(right), and as summarized in Table 2. Here emittance, energy spread, and bunch length are estimated in *normalized rms*, *rms relative*, and *rms*, respectively, and slice parameters before BC2 (after BC2) are estimated at ± 0.1 mm (± 0.02 mm) core region. In these simulations, we have included all important impedances such as space charge force in gun and X1 accelerating section, CSR and incoherent synchrotron radiation (ISR) in BCs, and short-range wakefields in all accelerating sections. According to our S2E simulations, all obtained slice parameters at the end of the linac are much better than our requirements as summarized in Table 2 and shown in Fig. 5. Here small spikes in current are generated by the weak over-compression at head and tail regions.

S2E SIMULATIONS ON JITTER

To relax jitter tolerance, we have adopted followings in PAL XFEL linac layout as shown in Fig. 1, where each accelerating section from X2 to K12 has four S-band accelerating columns: First, tight jitter tolerance can be improved by operating more klystrons in one accelerating section. Therefore one klystron will be dedicated to two sequent S-band accelerating columns from X1 to X5 sections to relax tight jitter tolerance there. Since X2AB (= X2A + X2B), X2CD, X3AB, and X3CD will be operated by their own klystrons under the same RF conditions, X2AB, X2CD, X3AB, and X3CD have the same jitter sensitivity [5]. Since jitter tolerance is loose at the downstream of BC2, one klystron will be dedicated to four sequent S-band accelerating columns from K2 to K12 sections. Second, tight jitter tolerance can be looser by operating S-band accel-

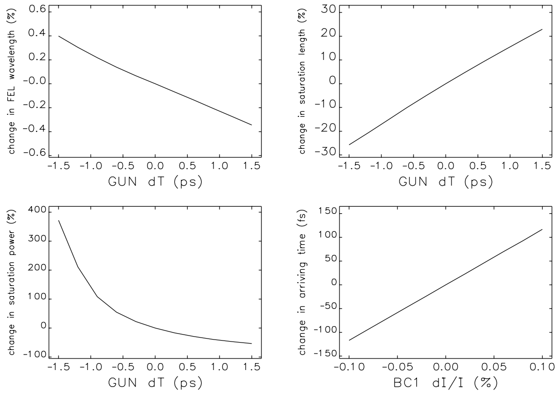

Figure 6: The most sensitive jitter sources in PAL XFEL linac: (top left) wavelength of FEL source versus gun timing jitter, (top right) saturation length versus gun timing jitter, (bottom left) saturation power versus gun timing jitter, and (bottom right) photon beam arriving time versus current error in BC1 magnet power supply.

erating columns around BCs with a low gradient of about 15 MV/m. To investigate the jitter sensitivity J_s and jitter tolerance J_t at the PAL XFEL linac, we have performed S2E simulations with ASTRA and ELEGANT codes. By applying an artificial jitter or error to each component, then by monitoring its impact on FEL performances, we can determine the jitter sensitivity of the component. In this paper, we assume that jitter is uncorrelated, and all components do not have any misalignment.

After considering users' requirements on photon beam stability, we have used following four constrains in determining the jitter sensitivity: First, peak-to-peak (p2p) change in wavelength of FEL source should be within ± 0.25%. Second, p2p change in saturation length should be within ± 5.0%. Third, p2p change in saturation power should be within ± 20.0%. Fourth, p2p change in bunch arriving time should be within ± 25 fs. The most sensitive jitter source in wavelength, saturation length, and saturation power is the gun timing jitter, and the most sensitive jitter source in bunch arriving time is the current error of magnet power supply for BC1 as shown in Fig. 6. Here the Ming Xie model is used in estimating FEL performances, which are averaged in 80% core slices.

By repeating above processes, we have determined jitter sensitivities and jitter tolerances of all linac components, which satisfy a relation of $\sqrt{\sum_{i=1}^{n}(J_{t,i}/J_{s,i})^2} < 1$, where n is the total number of all considered linac components. Investigated bunch-to-bunch jitter sensitivities and jitter tolerances are summarized in Table 3. Here Tol. (p2p) and Tol. (rms) are jitter tolerances which are estimated in *p2p* and *rms* respectively.

Recently, it was reported that gun timing jitter can be controlled within several tens of fs by newly developing laser-RF synchronizing and timing technologies, and by the help of newly developing advanced RF low level control system, rms phase error and rms voltage error can be controlled within 0.01 deg and 0.01%, respectively [13]. Therefore we expect that the PAL XFEL facility can supply stable FEL sources to users.

Table 3: Jitter sensitivity and tolerance at PAL XFEL.

Jitter parameter	Unit	Sensitivity	Tol. (p2p)	Tol. (rms)
gun timing ΔT	ps	-0.24	0.24	0.08
charge $\Delta Q/Q$	%	-3.00	3.00	1.00
X1AB $\Delta\phi$	deg	-0.14	0.06	0.02
X1AB $\Delta V/V$	%	-0.06	0.06	0.02
X2AB $\Delta\phi$	deg	-0.10	0.06	0.02
X2AB $\Delta V/V$	%	-0.11	0.06	0.02
X3X $\Delta\phi$	deg	+0.17	0.06	0.02
X3X $\Delta V/V$	%	+0.29	0.06	0.02
BC1 $\Delta I/I$	%	+0.02	0.02	0.007
X4AB $\Delta\phi$	deg	-0.64	0.06	0.02
X4AB $\Delta V/V$	%	-1.17	0.06	0.02
BC2 $\Delta I/I$	%	+0.11	0.02	0.007
K2 $\Delta\phi$	deg	-83.3	0.06	0.02
K2 $\Delta V/V$	%	+1.70	0.06	0.02

SUMMARY

By putting BC2 at a lower energy region, by using a short linac between BCs, and by choosing high compression factor at BC1, slice energy spread before BC2 is about 4.3×10^{-5}, which is large enough to control microbunching instability at BC2. In this case, optimized beam parameters at the end of PAL XFEL linac are also much better than our requirements, and growths of slice and projected normalized rms horizontal emittances in BCs are only 0.0 μm and 0.14 μm, respectively, even though peak current is about 4.0 kA. We expect that the PAL XFEL facility can supply stable FEL sources to users if jitter sources are controlled by newly developing advanced technologies.

REFERENCES

[1] L. H. Yu, Phys. Rev. A **44,** 5178 (1991).
[2] J. S. Oh, *et al.*, Nucl. Instr. and Meth. A **528,** (2004) 582.
[3] J. S. Oh, *et al.*, in these proceedings.
[4] J. Yang *et al.*, J. Appl. Phys. **92,** 1608 (2002).
[5] Yujong Kim *et al.*, in *Proc. EPAC2004*, 2004.
[6] Yujong Kim *et al.*, Nucl. Instr. and Meth. A **528,** (2004) 427.
[7] Yujong Kim *et al.*, in these proceedings.
[8] C. Travier, Nucl. Instr. and Meth. A **340,** (1994) 26.
[9] B.E. Carlsten, Nucl. Instr. and Meth. A **285**, (1989) 313.
[10] LCLS CDR, SLAC-R-593, 2002.
[11] Yujong Kim *et al.*, Nucl. Instr. and Meth. A **528,** (2004) 421.
[12] http://www.desy.de/∼yjkim/TESLA_S2E_2003_10.pdf
[13] S. Simrock, in *Proc. LINAC2004*, 2004.